

Panagiota I. Sarafoglou, Gregory N. Haidemenopoulos

Department of Mechanical Engineering, University of Thessaly, Volos, Greece

# Phase fraction mapping in the as-cast microstructure of extrudable 6xxx aluminum alloys

The mapping of  $Mg_2Si$  and  $\beta-AlFeSi$  phase fractions in the as-cast microstructure of Al–Mg–Si–Fe–Mn (6xxx series) alloys has been performed over the useful composition range (0–1.2 mass%) of the principal alloying elements Mg and Si. The calculations were based on the Scheil–Gulliver assumption of infinite diffusion in the liquid and limited diffusion in the solid state. The computed phase fractions were validated with experimental measurements of phase fractions. The mapping procedure allows the control of intermetallic phases in the as-cast microstructure, the minimization of the  $\beta-AlFeSi$  phase in particular, which is a significant prerequisite in obtaining enhanced extrudability, combined with high strength in this alloy series. Construction of maps for different levels of Mn has shown that addition of Mn could allow for higher alloying with Mg and Si, in order to obtain higher amounts of  $Mg_2Si$ , without at the same time increasing the  $\beta-AlFeSi$  phase in the as-cast microstructure.

**Keywords:** Aluminum alloys; Computational thermodynamics; Microsegregation; Alloy design

## 1. Introduction

In recent years there has emerged a growing need for the development of high-strength Al-alloy extruded profiles of complex shape for the needs of the transportation industry. This means that high strength should be combined with high extrudability in the 6xxx series alloys (Al–Mg–Si–Fe–Mn). The usual route followed so far is through increased alloying, for the formation of higher volume fractions of the strengthening  $Mg_2Si$  phase. At the same time this leads to the formation of higher volume fractions of Fe-bearing intermetallics,  $\alpha-Al_{12}(FeMn)_3Si$  and  $\beta-Al_5FeSi$ , from now on called  $\alpha-AlFeSi$  and  $\beta-AlFeSi$  respectively. The  $\alpha-AlFeSi$  has a cubic crystal structure and globular morphology while the  $\beta-AlFeSi$  possesses a monoclinic structure and a plate-like morphology, limiting the extrudability of the as-cast billet by inducing local cracking and surface defects in the extruded material [1]. To cope with these effects, prolonged homogenization treatments (up to 12 h just below the solidus temperature) are employed, after casting and prior to extrusion, in order to transform the  $\beta-AlFeSi$  to  $\alpha-AlFeSi$ , which has a much lesser impact on extrudability, raising the production cost substantially. This transformation has been investigated experimentally [2–7]

and by modeling [8, 9] and the effect of homogenization temperature and time in several alloys of the 6xxx series has been assessed. There has been less attention to the control of Fe-intermetallics in the as-cast microstructure, most important being the effect of cooling rate [5, 10, 11] and the dispersion of intermetallics in the microstructure [1, 12, 13]. However, a systematic methodology for the control of the intermetallic phases in the as-cast microstructure does not exist. In this work a methodology is presented, based on computational alloy thermodynamics, for the calculation of phase fractions of  $\beta-AlFeSi$  and  $Mg_2Si$ , as a function of the principal alloying elements in the 6xxx alloy series. The computed fractions are validated against experimental measurements of volume fractions in selected alloys. The fraction of  $Mg_2Si$  and  $\beta-AlFeSi$  is then mapped over the useful (up to 1.2 mass%) range in the Mg–Si composition space. These maps could be the first step towards the design of alloy compositions for enhanced extrudability-strength combinations.

## 2. Methodology

### 2.1. Computational method

All necessary thermodynamics calculations for the description of the Gibbs free energy of the various phases in the system were performed with the Thermo-Calc software [14], which is based on the CALPHAD approach [15]. For the Al–Mg–Si–Fe–Mn system under consideration the thermodynamic database for light non-ferrous alloys COST 507 [16] was used. This database was amended by recent thermodynamic descriptions [17, 18] of the intermetallic phases. The major phases in the Al–Mg–Si–Fe–Mn system are the liquid phase, the fcc matrix phase ( $\alpha-Al$ ), the intermetallic phases  $Mg_2Si$ ,  $\alpha-AlFeSi$ ,  $\beta-AlFeSi$ ,  $Al_{13}Fe_4$  and the Si-diamond phase. The  $Al_{13}Fe_4$  phase transforms to  $\beta-AlFeSi$  through a quasi-peritectic reaction  $L + Al_{13}Fe_4 = \beta-AlFeSi + \alpha-Al$  [19]. In addition, recent work [11, 20] has verified experimentally that  $Al_{13}Fe_4$  does not form in the as-cast microstructure. Based on the above, it was decided to exclude the  $Al_{13}Fe_4$  phase from the calculations. Solidification was assumed to take place under the condition of limited diffusion in the solid and infinite diffusion in the liquid (Scheil–Gulliver condition). This is a valid assumption since the diffusion coefficients of the alloying elements in the liquid phase are significantly larger than those in the solid phase. Phase fractions were then calculated with the

Scheil module of Thermo-Calc. It should be mentioned that other computational methods, which take into account macroscopic transport phenomena (melt flow and transport of crystals) have been developed for ternary alloys [21, 22]. However these methods use locally linearized phase diagrams and do not benefit, at the moment, from the available thermodynamic databases. After solidification the alloy is cooled to room temperature. In order to confirm if any further formation of  $\beta$ -AlFeSi phase takes place through the transformation of  $\alpha$  to  $\beta$ -AlFeSi during cooling from the solidus temperature, a kinetic calculation using the DICTRA software [23], with the most recent mobility database, has been performed. Details of these calculations are discussed in Section 3.3. The mapping of  $Mg_2Si$  and  $\beta$ -AlFeSi phase fractions is presented in Section 3.5.

### 2.2. Experimental procedure

In order to validate the results of the computations regarding the formation of intermetallic phases during solidification, three Al-alloy billets (6060, 6063 and 6082) were prepared industrially with direct-chill casting (AoG, Greece). The chemical composition of these alloys is listed in Table 1. The diameter of the billet was 200 mm and the solidification rate was  $2 \text{ mm s}^{-1}$ .

After solidification, the billets were sliced and specimens for metallographic preparation were cut in the transverse direction to the billet axis. Specimen preparation included cutting and grinding with SiC papers rating 120, 320, 500, 800, 1000 and 2400 grit. Polishing was performed with  $1 \mu\text{m}$  diamond paste followed by electro-polishing with BARKER'S reagent consisting of 10 ml fluoroboric acid (35%) and 200 ml water. The microstructure was revealed after etching in Keller's solution, consisting of 0.5% HF in 50 ml  $H_2O$  in order to reveal the intermetallic phases. Metallographic examination was carried out using an optical microscope (Leitz Aristomet, Germany). In order to compare the computed fractions of phases from the Scheil calculations, a quantitative determination of volume fractions was performed using image analysis methods, based on point counting, using a 1000 grit on 10 sections according to the ASTM E-562 standard [24]. The intermetallic phases were first identified in the scanning electron microscope (SEM) by determining their chemical composition by energy dispersive X-ray spectroscopy (EDS), (JEOL JSM-6510, Japan).

## 3. Results and discussion

### 3.1. Equilibrium calculations

Equilibrium calculations are presented in this section, which aim at identifying the major phases and their stability

Table 1. Chemical composition of aluminum alloys in the present study (in mass%).

Alloy	Al	Mg	Si	Fe	Mn
6060	Balance	0.48	0.4	0.2	0.03
6063	Balance	0.51	0.55	0.2	0.03
6082	Balance	0.9	0.63	0.2	0.45

limits in the alloys. For the 6060 alloy, the Si isopleth section for composition 0.48Mg, 0.03Mn and 0.2Fe (in mass%), is depicted in Fig. 1a. Similarly the Mg isopleth for 0.4Si, 0.03Mn and 0.2Fe (in mass%) is depicted in Fig. 1b. The  $Mg_2Si$  phase is stable bellow  $500 \text{ }^\circ\text{C}$ . The  $\alpha$ -AlFeSi phase is the first phase stabilized bellow the liquidus temperature. The range of stability of  $\alpha$ -AlFeSi extends to lower temperatures depending on Mg content. In contrast, Si stabilizes the  $\beta$ -AlFeSi phase. Additionally, the isopleths of Fig. 1 indicate that transformation of  $\alpha$  to  $\beta$ -AlFeSi takes place as the temperature drops below the solidus. For this reason as mentioned above, a kinetic calculation, described in Section 3.3, has been performed in order to determine the amount of  $\beta$ -AlFeSi phase, which forms after solidification.

An isothermal section of the Al–Mg–Si–Fe–Mn system at  $300 \text{ }^\circ\text{C}$ , and for 0.2Fe-0.03Mn (mass%) is shown in Fig. 2. In agreement with the above observations, Mg stabilizes the  $\alpha$ -AlFeSi phase up to 0.8 mass% Si and Si stabilizes the  $\beta$ -AlFeSi phase, which forms even for low concentrations of Mg and Si.

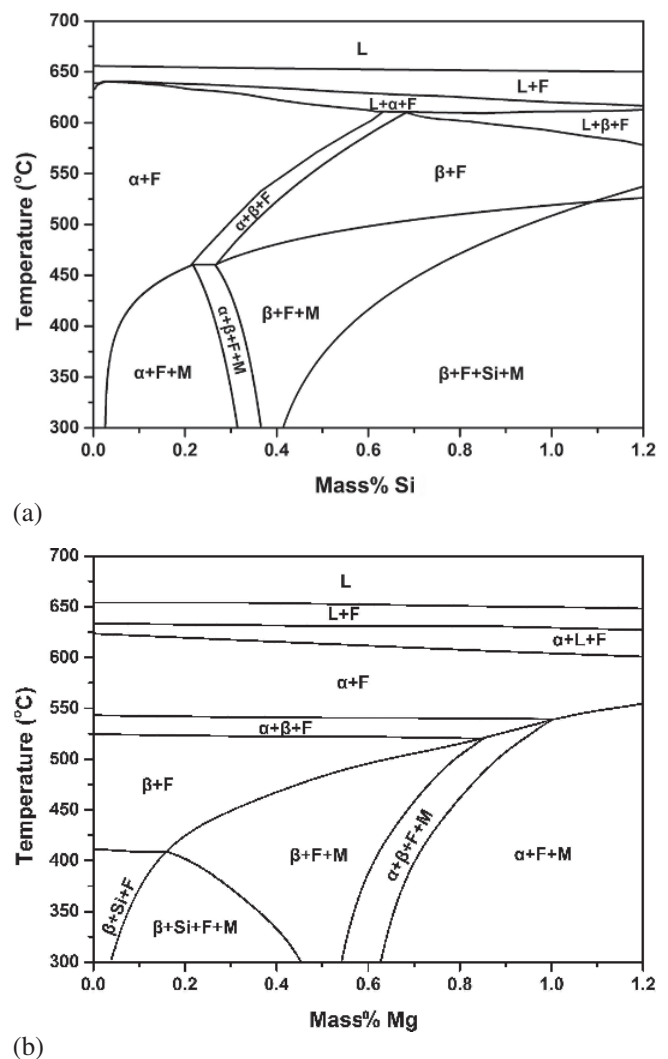


Fig. 1. (a) Si isopleth for 0.48Mg, 0.03Mn and 0.2 Fe (mass%) and (b) Mg isopleth for 0.4Si, 0.03Mn and 0.2 Fe (mass%) (L = liquid, F = fcc,  $\alpha$  =  $\alpha$ -AlFeSi,  $\beta$  =  $\beta$ -AlFeSi, M =  $Mg_2Si$ ).

### 3.2. Scheil microsegregation and phase fraction calculations

A typical Scheil solidification path, for the 6082-alloy with composition Al-0.9Mg-0.63Si-0.2Fe-0.45Mn (mass%) is shown in Fig. 3 as temperature vs mass fraction solid. The phase sequence during solidification is  $fcc \rightarrow \alpha\text{-AlFeSi} \rightarrow \beta\text{-AlFeSi} \rightarrow \text{Mg}_2\text{Si} \rightarrow \text{Si}$  (diamond). The arrows depict the temperature and the mass fraction of solid where each phase starts to form. The liquidus temperature for this alloy was calculated to be 652 °C and the solidus temperature is 550 °C.

The mole fraction of phases, formed during solidification, was calculated as a function of temperature and is shown in Fig. 4. Formation of  $\alpha\text{-AlFeSi}$  starts at 622 °C while further formation of  $\alpha\text{-AlFeSi}$  stops, when the  $\beta\text{-AlFeSi}$  starts to form at 588 °C. The  $\text{Mg}_2\text{Si}$  phase starts to form at 585 °C and continues to grow simultaneously with the  $\beta\text{-AlFeSi}$  phase until the quaternary eutectic temperature (554 °C) is reached and the remaining liquid transforms to a mixture of fcc,  $\beta\text{-AlFeSi}$ ,  $\text{Mg}_2\text{Si}$  and Si.

The phase fractions in the as-cast microstructure are  $4.14 \times 10^{-3}$   $\alpha\text{-AlFeSi}$ ,  $7.16 \times 10^{-4}$   $\beta\text{-AlFeSi}$ ,  $5.32 \times 10^{-3}$

$\text{Mg}_2\text{Si}$  and  $9.18 \times 10^{-4}$  Si-diamond. The above phases are not distributed uniformly in the microstructure but segregate to regions where the liquid solidifies last, i.e. close to grain boundaries. This phase segregation is depicted in Fig. 5a, which gives the mole fraction of all phases vs

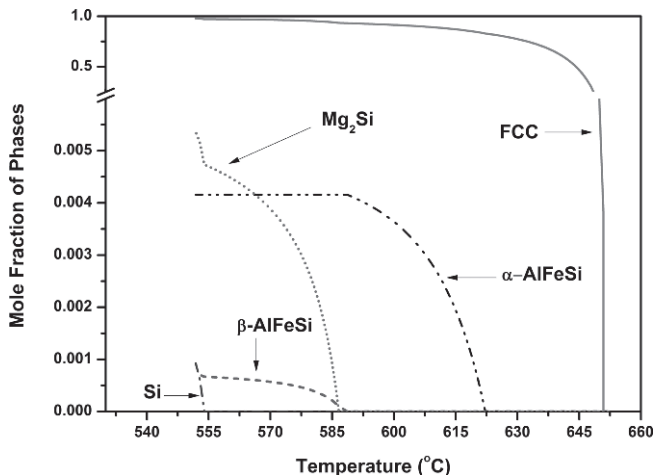


Fig. 4. Mole fraction of phases as a function of temperature during solidification of 6082 alloy.

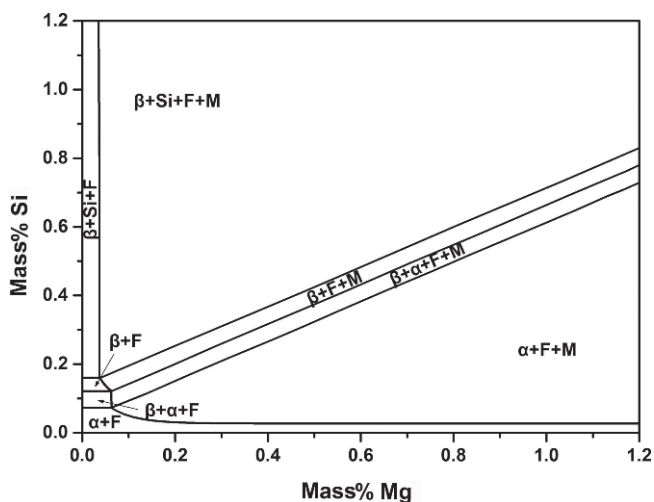


Fig. 2. Isothermal section of Al–Mg–Si with 0.2Fe-0.03Mn (mass%) at 300 °C, (L = liquid, F = fcc,  $\alpha$  =  $\alpha\text{-AlFeSi}$ ,  $\beta$  =  $\beta\text{-AlFeSi}$ , M =  $\text{Mg}_2\text{Si}$ ).

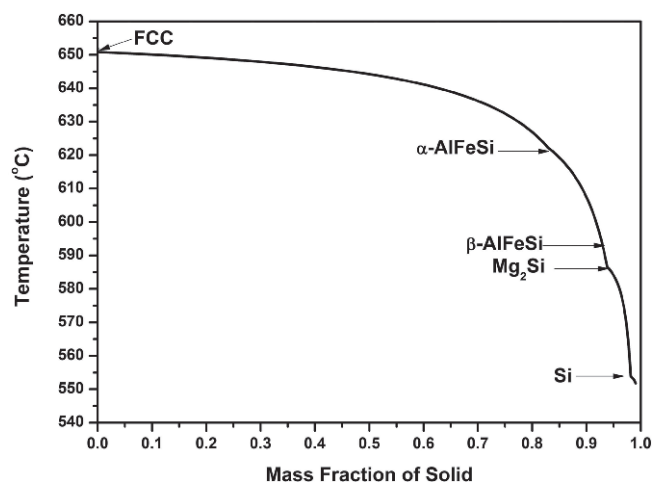
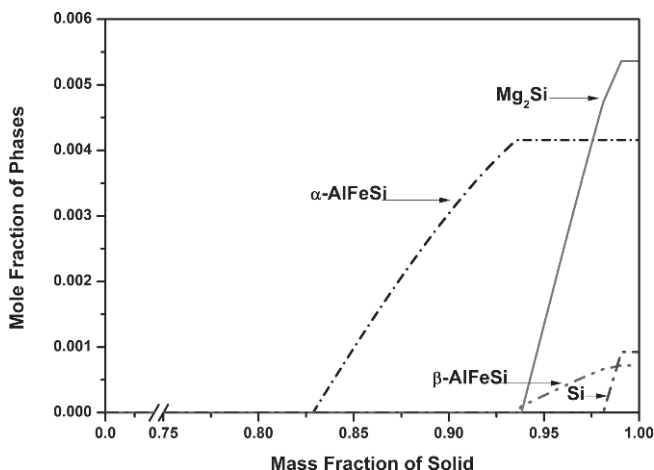
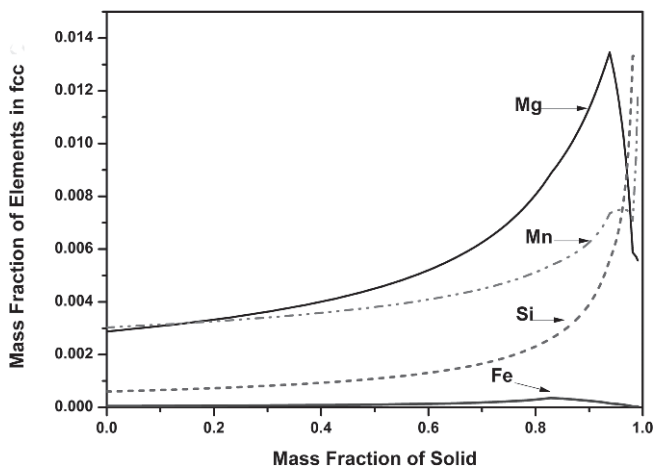


Fig. 3. Scheil solidification path for 6082 alloy.



(a)



(b)

Fig. 5. (a) Microsegregation of phases and (b) microsegregation of alloying elements of 6082 alloy during solidification.

fraction solid (fcc matrix is excluded). It is seen that the  $\alpha$ -AlFeSi phase forms above 85% solidification while all other phases form above 95% solidification. This means that the intermetallic phases form at the secondary dendrite boundaries towards the end of solidification. Accordingly the microsegregation of the alloying elements in the fcc matrix follows a similar trend, i.e. increase towards the end of solidification, as shown in Fig. 5b. The drop in the concentration profile of Mg and Fe is attributed to the formation of  $Mg_2Si$  and iron intermetallics respectively.

### 3.3. Transformation of $\alpha$ to $\beta$ -AlFeSi after solidification

The Scheil simulation described above defines the phase fractions present in the microstructure at the end of solidification. According to the isopleth sections in Fig. 1 transformation of  $\alpha$  to  $\beta$ -AlFeSi takes place below the solidus temperature during equilibrium cooling. However, taking into account the high cooling rates of the solidified ingots, following the direct-chill casting operation, it should be evaluated whether this transformation produces any appreciable amount of  $\beta$ -AlFeSi phase. A kinetic simulation using the DICTRA computational kinetics software was performed for the 6082 alloy. The geometric model used in a previous work [7] was employed and is shown in Fig. 6. The calculation domain consists of two regions. The first region corresponds to the fcc matrix phase while the  $\alpha$ -AlFeSi is taken as a dispersed spheroidal phase. The second region was attached to the right of the first region and corresponds to the  $\beta$ -AlFeSi phase. The width of the fcc region was taken to be one half of the mean secondary dendrite arm spacing ( $10\ \mu m$ ) and the width of the  $\beta$ -AlFeSi corresponded to the mole fraction of the  $\beta$ -AlFeSi as calculated by the Scheil simulation. For the composition of the 6082 alloy, the mole fraction of  $\beta$ -AlFeSi corresponds to a width of the  $\beta$ -AlFeSi region equal to  $0.0111\ \mu m$ . The temperature during the simulation was considered to drop from 600 to 200 °C in 1 h corresponding to a cooling rate of  $0.11\ K\ s^{-1}$ . In order to take into account the impeding effect of the dispersed  $\alpha$ -AlFeSi phase on the diffusivities of the elements in the fcc matrix phase, a labyrinth factor [25], taken equal to the volume fraction of the  $\alpha$ -AlFeSi phase [26] was employed. The result of the simulation is given in Fig. 7, which shows the position of fcc/ $\beta$ -AlFeSi interface as a function of simulation (cooling) time. The final position of the interface at  $9.99977\ \mu m$ , to the left of the initial position ( $10\ \mu m$ ), corresponds to an increase of the volume fraction of  $\beta$ -AlFeSi

phase by 2.07% of the amount of  $\beta$ -AlFeSi formed during solidification. This value is considered negligible and therefore the amount of the  $\beta$ -AlFeSi phase, used for the construction of the maps in Section 3.5, was taken directly from the Scheil simulations.

### 3.4. Experimental validation of the computed phase fractions

The purpose of this section is to provide the necessary experimental data, regarding the fractions of phases, for the validation of the computational methodology used in this work. Due to the difficulties encountered when measuring low volume fractions, the work was performed mainly on alloy 6082, which because of the higher alloy content, possessed a higher volume fraction of intermetallic phases. The following methodology was applied: first the phases were identified using SEM combined with EDS analysis and then a correspondence between SEM and optical microscopy was established in order to identify the phases in optical micrographs. This methodology enabled the use of a point counting method in order to determine the volume fractions of phases, using a high number of metallographic sections at the lowest magnification possible in order to get the most representative microstructure.

The as-cast microstructure of 6082 is depicted in the SEM micrograph Fig. 8. The EDS signal from areas 1 and

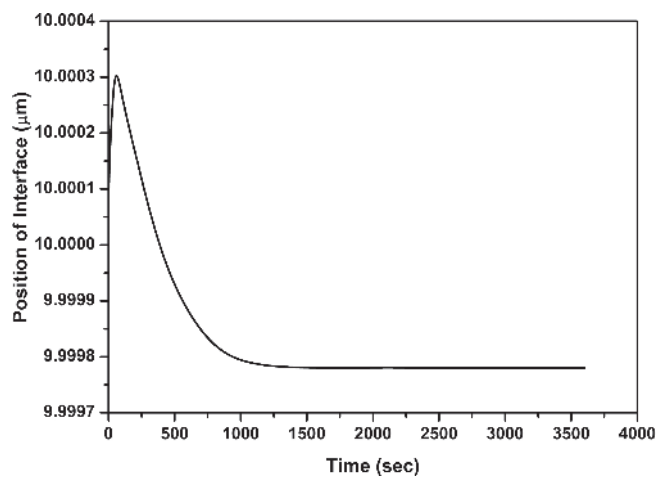


Fig. 7. Position of fcc/ $\beta$ -AlFeSi interface with simulation (cooling) time during cooling from 600 to 200 °C of 6082 alloy.

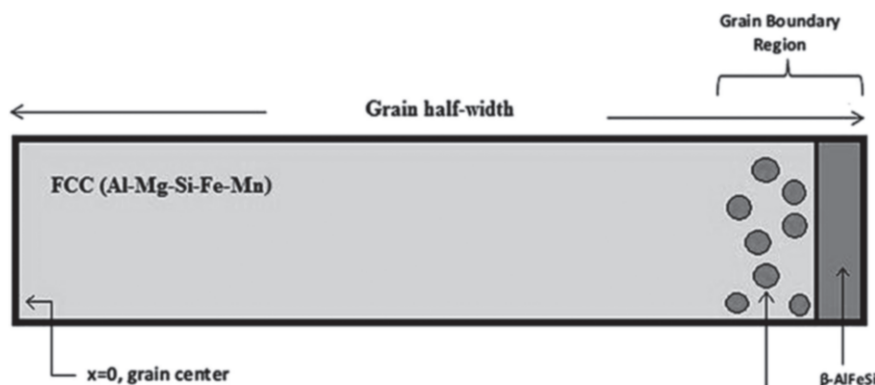


Fig. 6. Geometric model for the simulation of the  $\alpha \rightarrow \beta$ -AlFeSi transformation during cooling of 6082 alloy.

2 consisted of Mg and Si indicating that this phase is  $Mg_2Si$ . The signal from area 3 consisted of Al, Fe, Si and Mn indicating that it is the  $\alpha$ -AlFeSi phase, which contains Mn. The signal from area 4 consisted of Al, Fe and Si (without Mn) and was identified as  $\beta$ -AlFeSi. In order to further verify the phase identification, the composition of the  $\alpha$ -AlFeSi was determined quantitatively. It should be mentioned that the interaction area of the EDS measurement performed in this work was about  $1 \mu m^2$  while the average size of  $\alpha$ -AlFeSi particles on which the EDS signal was taken was  $20-30 \mu m^2$ . The results are listed in Table 2 and compared with measured literature data [12, 27–29]. The measured composition of  $\alpha$ -AlFeSi lies within the range reported in the literature and, therefore, the phase can be identified as  $\alpha$ -AlFeSi.

The SEM phase identification was then correlated with optical micrographs. The microstructure of the as-cast 6060, 6063 and 6082 aluminum alloys is depicted in Fig. 9a–c respectively and consists of Al-rich solid solution dendrites while the intermetallic phases are segregated at the secondary dendrite arm boundaries. These phases are identified as  $Mg_2Si$  (black),  $\alpha$ -AlFeSi (gray plate-like with rounded edges) and  $\beta$ -AlFeSi (gray plate-like). These observations are also in very good qualitative agreement with available metallographic observations in the literature [1, 12, 30].

The Scheil simulation on 6082 (Fig. 4) indicated that the last liquid solidifies by a quaternary eutectic consisting of fcc +  $\beta$ -AlFeSi +  $Mg_2Si$  + Si. The amount of this quaternary eutectic is small compared with the primary phases

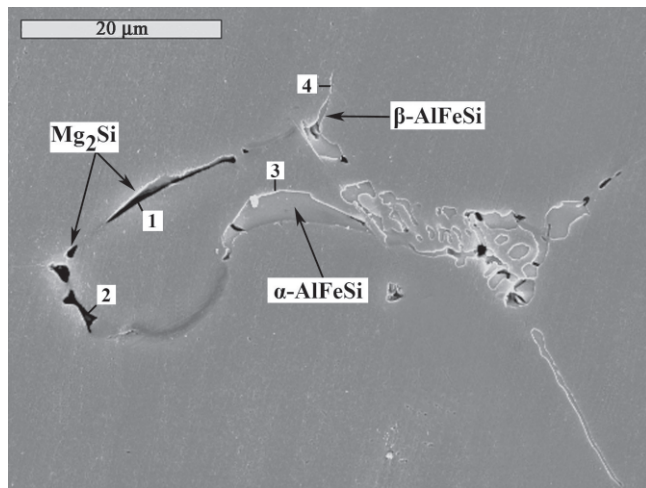
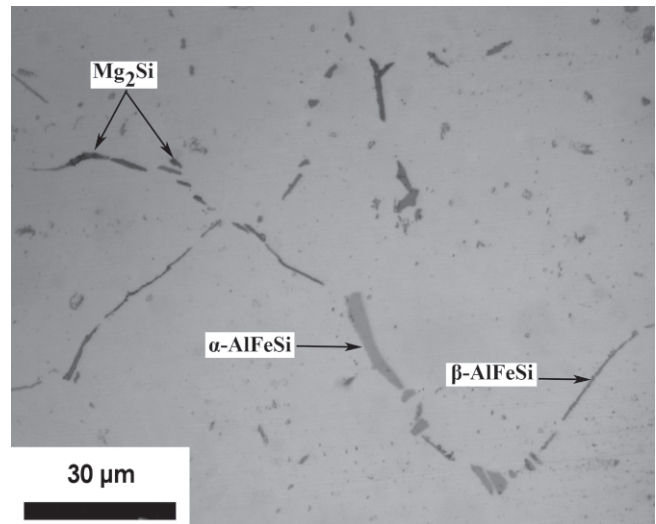


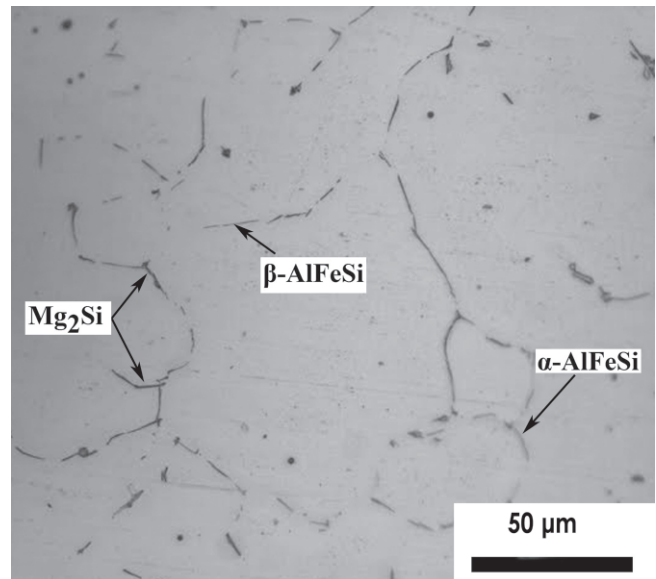
Fig. 8. SEM micrograph of the as-cast microstructure of 6082 Al-alloy indicating  $\alpha$ -AlFeSi,  $\beta$ -AlFeSi and  $Mg_2Si$  phases and position of EDS signals.

Table 2. Chemical composition of  $\alpha$ -AlFeSi phase (mass%).

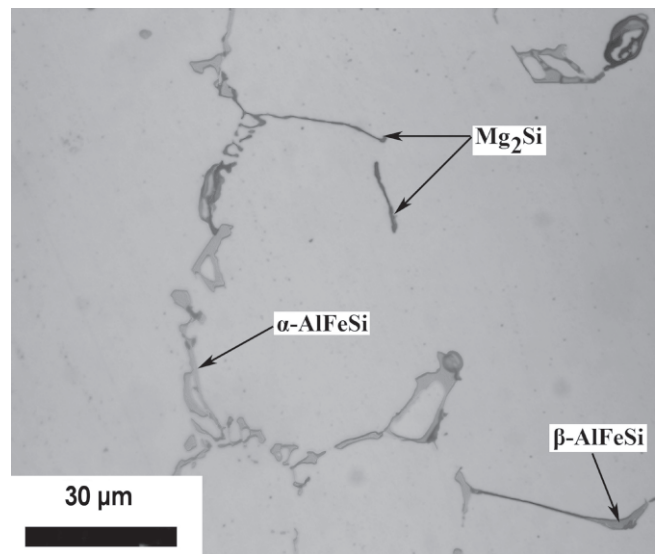
Phase	Si	Fe	Mn	Reference
$\alpha$ -AlFeSi	8–12	11–13	14–20	[12]
	10–12	10–15	15–20	[27]
	5.5–6.5	5.1–27.9	14–24	[28]
	5–7	10–13	19–23	[29]
	6.3–11.5	7.4–14.3	5.5–9.8	This work



(a)



(b)



(c)

Fig. 9. Optical micrographs of as-cast microstructures of (a) 6060, (b) 6063, (c) 6082 alloys.

and forms when less than 10 % liquid remains, in agreement with Ref. [30]. This quaternary eutectic cluster can be seen in Fig. 10.

Scheil calculations of phase fractions are compared with experimental measurements in Table 3 for  $\alpha$ -AlFeSi,  $Mg_2Si$  and quaternary eutectic (fcc +  $Mg_2Si$  +  $\beta$ -AlFeSi + Si). Taking into account the experimental error involved when measuring low volume fractions, the agreement between the Scheil simulation predictions and the experimental measurements is considered satisfactory. Therefore computed fractions from the Scheil simulations were used for the phase fraction mapping of intermetallic phases in the as-cast microstructure.

### 3.5. Mapping of intermetallic phases

Alloys 6060 and 6063 contain 0.03 mass% Mn while alloy 6082 contains 0.45 mass% Mn. Therefore, Scheil calculations for phase fraction mapping were conducted for these two Mn levels. The mole fraction of  $\beta$ -AlFeSi and  $Mg_2Si$ , is depicted in the contour plots of fixed mole fractions in Fig. 11a and b respectively as a function of Mg and Si content for the two Mn levels of 0.03 and 0.45 mass%. The mole fraction of the  $\beta$ -AlFeSi phase decreases towards the lower right corner of the contour plot, indicating that low  $\beta$ -AlFeSi can be obtained at lower Si and higher Mg contents. The 0.45 % Mn iso- $\beta$  lines lie above the respective 0.03 % Mn iso- $\beta$  lines, indicating that for fixed Mg content, higher Mn allows the use of higher Si, without further increase of  $\beta$ -AlFeSi (Si stabilizes  $\beta$ -AlFeSi). The spacing

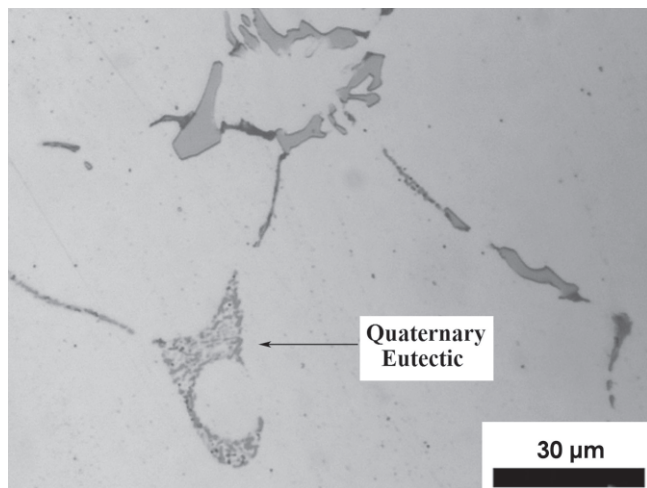
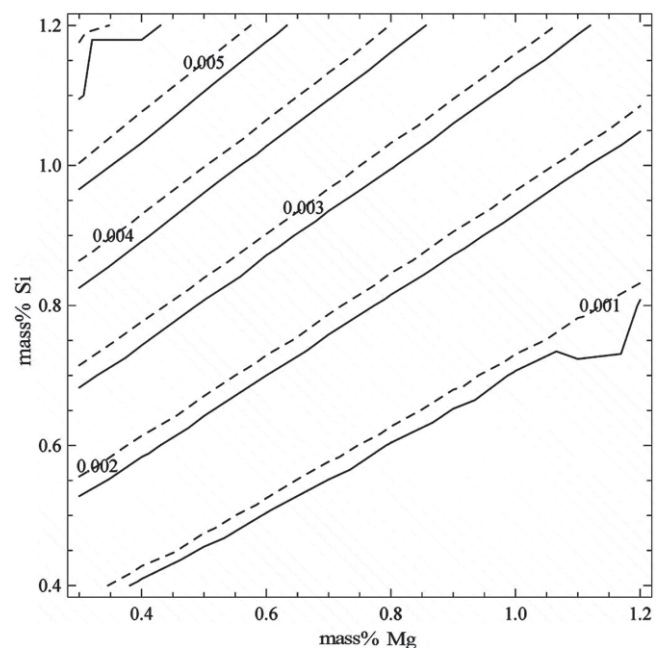


Fig. 10. The quaternary eutectic consisting of fcc +  $\beta$ -AlFeSi +  $Mg_2Si$  + Si in the as-cast microstructure of 6082 alloy.

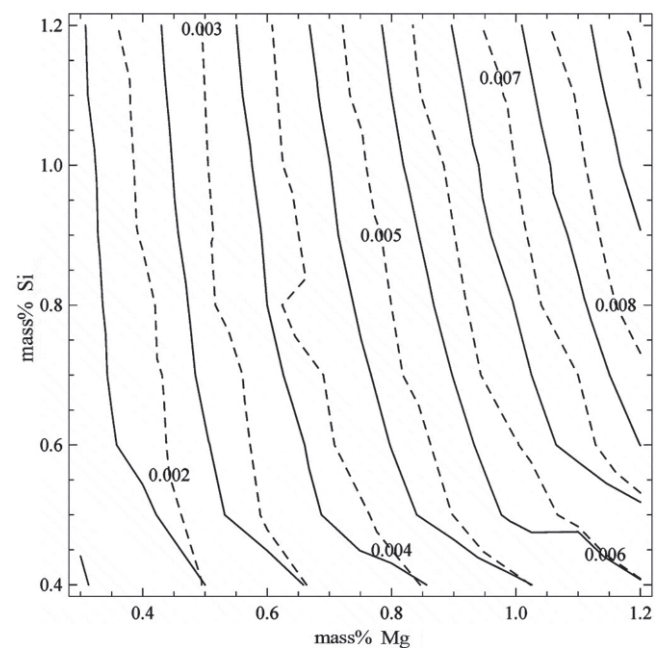
Table 3. Measured volume fractions of  $\alpha$ -AlFeSi,  $Mg_2Si$  and quaternary eutectic compared with simulation predictions for the 6082 aluminum alloy.

	Calculated ( $\times 10^{-3}$ )	Measured ( $\times 10^{-3}$ )
$\alpha$ -AlFeSi	4.14	4.2
$Mg_2Si$	5.32	3.65
Quaternary eutectic	3.8	4.1

between the iso- $\beta$  lines for the two Mn levels increases towards the upper left corner of the contour plot, indicating that the effect of Mn (in reducing  $\beta$ -AlFeSi) becomes stronger at higher Si and lower Mg contents. Regarding the  $Mg_2Si$  phase (Fig. 11b) it is clear that the mole fraction increases towards the upper right corner of the contour plot, indicating that an increase of both Mg and Si results in an increase of  $Mg_2Si$ , with Mg having a stronger effect. The 0.45 % Mn iso- $Mg_2Si$  lines lie above the 0.03 % Mn lines, indicating that a higher Mg content is required to obtain the same  $Mg_2Si$  mole fraction in the microstructure.



(a)



(b)

Fig. 11. Contour plots (maps) of fixed mole fractions of (a)  $\beta$ -AlFeSi and (b)  $Mg_2Si$  phases in the as-cast microstructure of Al-Mg-0.2Fe-Mn alloys (full lines 0.03 Mn, dotted lines 0.45 Mn, mass%).

Mapping of both the  $Mg_2Si$  phase and the  $\beta-AlFeSi$  phase across the Mg–Si space can be very useful for alloy design purposes. Such maps are shown in Fig. 12a and b for the two Mn levels of 0.03 and 0.45 % Mn respectively. The mole fractions of the  $\beta-AlFeSi$  phase range from 0.001 to 0.005 while those for the  $Mg_2Si$  range from 0.002 to 0.009. The position of alloys 6060, 6063 and 6082 is also indicated on the maps. All three alloys possess a low fraction of  $\beta-AlFeSi$  indicating an excellent extrudability potential. In addition, the 6082 alloy possesses a higher fraction of  $Mg_2Si$  indicating a higher strength potential compared to 6060 and 6063. The  $Mg_2Si$  is maximized to-

wards the upper right corner while the  $\beta-AlFeSi$  phase is minimized towards the lower right corner of the maps. This allows selection of optimum compositions for favorable as-cast microstructures in terms of the two phases. The Mn effect can be summarized as the potential to move to higher Mg and Si compositions in order to obtain higher amount of  $Mg_2Si$  without at the same time increasing the  $\beta-AlFeSi$  phase in the as-cast microstructure.

#### 4. Conclusions

From the results presented in this work, it can be deduced that the variation of the mole fractions of the extrudability-limiting  $\beta-AlFeSi$  phase and the strengthening  $Mg_2Si$  phase with alloying elements can be mapped over the useful range (0–1.2 mass%) in the Mg–Si composition space. The constructed maps indicate that low mole fractions of  $\beta-AlFeSi$  are associated with lower Si and higher Mg compositions. On the other hand, high mole fractions of  $Mg_2Si$  are associated with both higher Si and Mg compositions, with Mg possessing a stronger effect. Construction of maps for different levels of Mn has shown that addition of Mn could allow for higher alloying with Mg and Si, in order to obtain higher amounts of  $Mg_2Si$ , without at the same time increasing the  $\beta-AlFeSi$  intermetallic phase in the as-cast microstructure.

This work has been performed in the framework of cooperation with Aluminum of Greece (AoG). The authors are grateful to H. Kamoutsi, G. Tsantidis and N. Tzumaka for their assistance in the preparation of the plots.

#### References

- [1] Y.L. Liu, S.B. Kang: *J. Mater. Sci.* 32 (1997) 1443–1447. DOI:10.1023/A:1018545732009
- [2] M. Cai, J.D. Robson, G.W. Lorimer, N.C. Parson: *Mater. Sci. Forum* 396–402 (2002) 209–214. DOI:10.4028/www.scientific.net/MSF.396-402.209
- [3] N.C.W. Kuijpers: Kinetics of the  $\beta-AlFeSi$  to  $\alpha-Al(FeMn)Si$  transformation in Al–Mg–Si alloys, Ph.D. Thesis, TU Delft, 2004.
- [4] S. Onurlu, A. Tekin: *J. Mater. Sci.* 29 (1994) 1652–1655. DOI:10.1007/BF00368940
- [5] H. Tanihata, T. Sugawara, K. Matsuda, S. Ikeno: *J. Mater. Sci.* 34 (1999) 1205–1210. DOI:10.1023/A:1004504805781
- [6] O. Engler, Z. Liu, K. Kuhnke: *J. Alloys Compd.* 560 (2013) 111–122. DOI:10.1016/j.jallcom.2013.01.163
- [7] O. Engler, G. Lapyteva, N. Wang: *Mater. Charact.* 79 (2013) 60–75. DOI:10.1016/j.matchar.2013.02.012
- [8] N.C.W. Kuijpers, F.J. Vermolen, K. Vuik, S. van der Zwaag: *Mater. Trans.* 44 (2003) 1448–1456. DOI:10.2320/matertrans.44.1448
- [9] G.N. Haidemenopoulos, H. Kamoutsi, A.D. Zervaki: *J. Mater. Process. Technol.* 212 (2012) 2255–2260. DOI:10.1016/j.jmatprotec.2012.06.026
- [10] W.D. Fei, S.B. Kang: *J. Mater. Sci. Lett.* 14 (1995) 1795–1797. DOI:10.1007/BF00271010
- [11] A. Verma, S. Kumar, P.S. Grant, K.A.Q. O’Reilly: *J. Alloys Compd.* 55 (2013) 274–282. DOI:10.1016/j.jallcom.2012.12.077
- [12] G. Mrowka-Nowotnik, J. Sieniawski, M. Wierzbinska: *Arch. Mater. Sci. Eng.* 28 (2007) 69–76.
- [13] A. Wimmer, J. Lee, P. Schumacher: *Berg- Huttenmann. Monatsh.* 157 (2012) 301–305. DOI:10.1007/s00501-012-0034-7
- [14] J.O. Andersson, T. Helander, L. Höglund, P. Shi, B. Sundman: *Calphad* 26 (2002) 273–312. DOI:10.1016/S0364-5916(02)00037-8
- [15] H.L. Lukas, S.G. Fries, B. Sundman: *Computational thermodynamics, the Calphad method*, Cambridge University Press (2007). DOI:10.1017/CBO9780511804137
- [16] J. Ansara, A.T. Dinsdale, M.H. Rand: *COST 507 Thermochemical database for light metal alloys*, European Community publication 2, EUR 18449 (1991).

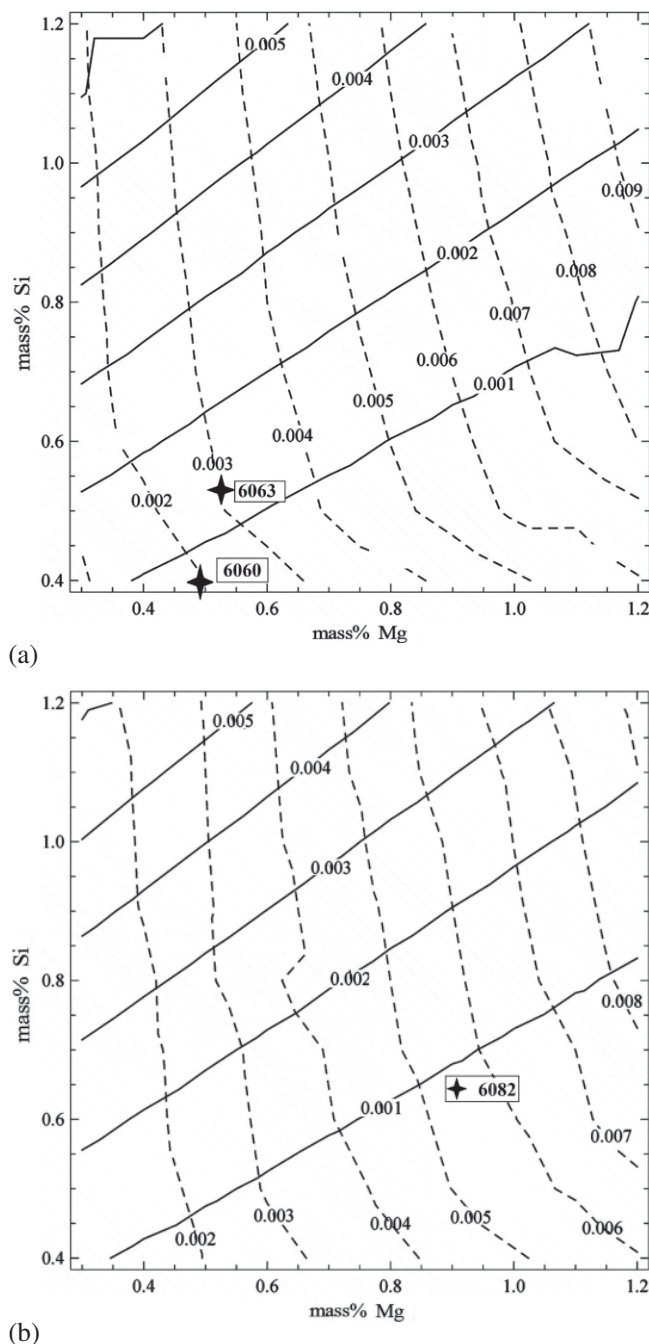


Fig. 12. Contour plots (maps) of fixed mole fractions  $\beta-AlFeSi$  (solid lines) and  $Mg_2Si$  (dotted lines) in as-cast microstructure of Al–Mg–Si–0.2Fe–Mn alloys for (a) 0.03 Mn and (b) 0.45 Mn, mass%. Compositions for alloys 6060, 6063 and 6082 are indicated on the maps.

- [17] Y. Du, Y.A. Chang, S.D. Liu, B.Y. Huang, F.Y. Xie, Y. Yang, S.L. Chen: *Z. Metallkd.* 96 (2005) 1351–1362.  
DOI:10.3139/146.101185
- [18] J. Lacaze, L. Eleno, B. Sundman: *Metall. Mater. Trans. A* 41 (2010) 2208–2215. DOI:10.1007/s11661-010-0263-x
- [19] G. Sha, K.A.Q. O'Reilly, B. Cantor, J.M. Titchmarsh, R.G. Hamerton: *Acta Mater.* 51 (2003) 1883–1897.  
DOI:10.1016/S1359-6454(02)00595-5
- [20] T. Smith, K.A.Q. O'Reilly, S. Kumar, I. Stone: *Metall. Mater. Trans. A* 44 (2013) 4866–4871.  
DOI:10.1007/s11661-013-1934-1
- [21] M. Wu, A. Ludwig: *Metall. Mater. Trans. A* 38 (2007) 1465–1475. DOI:10.1007/s11661-007-9175-9
- [22] M. Wu, J. Li, A. Ludwig, A. Kharicha: *Comput. Mater. Sci.* 79 (2013) 830–840. DOI:10.1016/j.commatsci.2013.05.015
- [23] A. Borgenstam, L. Höglund, J. Ågren, A. Engström: *J. Phase Equilib.* 21 (2000) 269–280.  
DOI:10.1361/105497100770340057
- [24] ASTM E-562 Specification, Standard Test Method for Determining Volume Fraction by Systematic Manual Point Count, American Society for Testing and Materials, PA, USA (2003).
- [25] J.W. Rayleigh: *Philos. Mag.* 34 (1892) 481–502.  
DOI:10.1080/14786449208620364
- [26] W. Zhang, Y. Du, Y. Peng, G. Wen, S. Wang: *Int. J. Refract. Met. Hard Mater.* 104 (2013) 721–735.
- [27] L.F. Mondolfo: *Aluminum Alloys: Structure and Properties*, Butterworths, London-Boston (1976).  
DOI:10.1016/B978-0-408-70932-3.50032-2
- [28] M. Warmuzek, K. Rabczak, J. Sieniawski: *J. Mater. Process. Technol.* 175 (2006) 421–426.  
DOI:10.1016/j.jmatprotec.2005.04.005
- [29] Y.L. Liu, S.B. Kang, H.W. Kim: *Mater. Lett.* 41 (1999) 267–272.  
DOI:10.1016/S0167-577X(99)00141-X
- [30] Y. Birol: *Mater. Charact.* 73 (2012) 37–42.  
DOI:10.1016/j.matchar.2012.07.015

(Received May 15, 2014; accepted July 25, 2014; online since September 30, 2014)

#### Correspondence address

Professor Gregory N. Haidemenopoulos  
Department of Mechanical Engineering  
University of Thessaly  
Volos 38334  
Greece  
Tel.: +30 2421074062  
Fax: +30 2421074061  
E-mail: hgreg@mie.uth.gr

#### Bibliography

DOI 10.3139/146.111139  
*Int. J. Mater. Res. (formerly Z. Metallkd.)*  
105 (2014) 12; page 1202–1209  
© Carl Hanser Verlag GmbH & Co. KG  
ISSN 1862-5282